Nuclear Science and Techniques (2026) 37:15
https://doi.org/10.1007/s41365-025-01807-z

Sensitivity analysis of rod rearrangement in criticality safety for PWR fuel assemblies under transportation accidents

Xin-Ling Dai[1] · De-Chang Cai[2] · Yan-Min Zhang[1] · Jin Cai[2]

Received: 28 May 2024 / Revised: 30 July 2024 / Accepted: 7 August 2024 / Published online: 7 December 2025

Abstract
To ensure the safe transportation of radioactive materials, numerous countries have established specific standards. For the transfer of fissile materials, it is imperative that the material within the packaging remains in a subcritical state during routine, normal, and accidental transport conditions. In the event of an accident, the rods within the storage tank may become rearranged, introducing uncertainty that must be accounted for to ensure that criticality analysis results are conservative. Historically, this uncertainty was addressed overly conservatively due to limited research on non-uniform arrangement scenarios, which proved unsuitable for criticality safety analysis of spent fuel packages. This paper introduced three distinct methods to non-uniformly rearrange fuel rods—Uniform Arrangement by Blocks, Layer-by-Layer Determination, and Birdcage Deformation—and meticulously evaluates the influences of rod rearrangement on the effective multiplication factor of neutrons, k_{eff}, utilizing the Monte Carlo method. Ultimately, this study presents a holistic method capable of encompassing the entire spectrum of potential effects stemming from the rearrangement of fuel rods during rods mispositioning accident. By augmenting the safety margin, this approach proves to be adeptly suited for the criticality safety analysis of nuclear fuel transport containers.

Keywords Criticality safety analysis · Fuel transports · Rods mispositioning accident · Non-uniform arrangement

1 Introduction

Nuclear energy, recognized for its cleanliness, low-carbon footprint, safety, and efficiency, stands as a fundamental load energy source that is instrumental in combating global climate change [1]. In the wake of the Fukushima nuclear disaster, the international community has been compelled to adopt new safety standards that are more rigorous and exacting. Among these standards, ensuring the secure transportation of radioactive materials has emerged as a paramount concern, essential for the protection of public health and safety [2]. In response to this imperative, the International Atomic Energy Agency (IAEA), in conjunction with a multitude of nations, has crafted detailed laws and regulations specifically designed to govern the transportation of radioactive material packages [3, 4].

The swift advancement of China's nuclear technology sector necessitates the transportation of substantial volumes of radioactive materials [5]. Central to this process is the transport container, which serves as the pivotal apparatus for the secure conveyance of nuclear fuel assemblies from the component fabrication facility to the reactor site. It is imperative that these containers maintain the structural integrity of their contents [6–8], while also ensuring that the criticality safety and shielding effectiveness of the packages adhere to the stipulated regulatory standards throughout the transportation phase [9]. The regulations stipulated in Ref. [4] dictate that transport containers for radioactive materials must be designed with the capacity to securely retain their contents even in the event of a transportation accident. Prior to their deployment, transport packages are required to fulfill the criteria outlined in preceding legislation [10]. For instance, both the type RY-I spent fuel transport packages [11] and the type FCo70-YQ medical radioactive source transport packages [12] underwent a series of rigorous tests before being

✉ De-Chang Cai
caidechang@cgnpc.com.cn

[1] Institute of Nuclear and New Energy Technology, Tsinghua University, Beijing 100084, China

[2] China Nuclear Power Technology Research Institute Co Ltd, Shenzhen 518000, China

approved for service. Notably, as specified in reference [4], for packages intended to carry fissile materials, an additional criticality safety analysis is mandated [13]. This analysis is of paramount importance, as it verifies that the fissile material remains subcritical under a range of conditions, including conventional, normal, and accidental scenarios [4]. The criticality analysis must also encompass abnormal scenarios that could potentially impact the system's effectiveness, such as the ingress of water into the container or the failure of neutron absorber elements during an accident. These atypical conditions could lead to an increase in the effective multiplication factor, k_{eff}, of the evaluated system [14–17]. It is imperative that the criticality analysis provides an assessment of the uncertainty associated with the calculation results, enabling a robust evaluation of the system's safety [18]. This requirement is further underscored by the guidelines on nuclear criticality safety for fissile materials outside of reactors, as detailed in reference [19]. To ascertain this uncertainty, it is essential to take into account the potential deformation of the fuel elements under accidental conditions, as these factors can significantly influence the overall safety assessment.

The safety analysis of nuclear fuel assembly transport containers necessitates a dual approach encompassing both mechanical and criticality safety analyses [20]. A variety of methodologies are employed for mechanical analysis, including isotropic modeling, scaled modeling, and finite element analysis [21, 22]. Studies presented in Ref. [23, 24] conducted a series of drop tests on the RA-3D model packages to simulate the cumulative effects of the most severe drop accident scenarios on the fuel elements. The findings from these studies indicate that compliant transport packagings offer substantial protection to the fuel assembly contained within. Despite significant deformation on the exterior of the impacted transport packaging, the fuel assembly remains structurally sound. While fuel rods may bend and interim spacers may deform, the integrity of the fuel rod cladding is preserved, preventing any leakage of fissile material from the interior. Beyond the RA-3D packages, transport containers for fuel assemblies are invariably designed with cushioning mechanisms for added protection. For instance, the Tianwan nuclear fuel assembly transport containers incorporate wire rope vibration isolators, which significantly dampen the vibrations experienced during transport [25]. Consequently, under accident conditions, the focus should shift from the potential breakage of fuel cladding to the alteration in the pitch between fuel rods. This alteration, also referred to as lattice expansion, represents a significant factor in the fuel relocation effect, which has implications for criticality safety [26].

This paper presents a simplified approach to the fuel deformation issue by reducing it to a single-variable problem, specifically focusing on the sensitivity of critical safety analysis to variations in rod pitch. Consequently, the paper posits that the pitch of fuel rods varies across the active zone. As demonstrated in the reference [27], even under the most severe drop conditions, the area of fuel rod buckling is localized near the point of impact and does not extend throughout the entire active region of the fuel assembly. This implies that only a segment of the fuel rods is likely to exhibit deformation that could potentially increase reactivity. Thus, the strategy of uniformly adjusting the fuel rod pitch across the entire active zone is considered a conservative approach.

As highlighted in reference [13], it is imperative to address abnormal conditions, such as water ingress into the package and the failure of interim spacers, with particular scrutiny. X. Wang et al. conducted a comprehensive investigation into the impact of uniform variations in fuel rod pitch within the AP1000 fresh fuel transportation vessel, as well as the effects of water ingress on criticality safety, utilizing the Monte Carlo N-Particle (MCNP) code [28]. Initially, they examined the uniform expansion of fuel rod pitch within the storage cavity of the transport container. Their findings revealed that the k_{eff} reaches its peak when the fuel rods uniformly occupy the storage cavity. Subsequently, they explored the influence of water ingress with varying densities into the cargo package on criticality safety. The study's outcomes indicated that the criticality safety is most compromised when the fuel assembly within the cargo package is entirely submerged in water with a density of 1×10^3 kg/m^3.

Historically, the China Nuclear Power Technology Research Institute Co., Ltd. (CNPRI) has incorporated an additional uncertainty of 4,000 pcm into the criticality safety analysis for fresh fuel transportation containers, in addition to the conditions where fuel assemblies are submerged and the fuel rods uniformly occupy the storage cavities. As demonstrated in the paper [29], spent fuel transportation casks are required to accommodate dozens of fuel assemblies, and the existing safety margin is inherently limited [30]. Consequently, the methodology previously employed by CNPRI is deemed unsuitable for the criticality safety analysis of spent fuel transport packages, given the heightened requirements and complexities associated with the transportation of spent fuel.

However, accurately quantifying this uncertainty presents a challenge due to the existing gaps in prior research concerning the arrangement of fuel rods. Moreover, the majority of these studies have been predicated on the assumption of a uniform arrangement of fuel rods. To date, the non-uniform arrangement of fuel rods has only been examined in a limited number of publications, specifically:

a. S. Whittingham et al. determined the non-uniform arrangement of fuel rods when k_{eff} takes the maximum value by expanding the fuel rods layer by layer [31].

b. M. Asami et al. developed a mathematical model based on the possible Birdcage Deformation of the fuel rods during a drop accident. The non-uniform arrangement of fuel rods is regulated by parameterizing the radius of curvature during lower nozzle deformation [32].

This paper undertakes a comprehensive investigation of the non-uniform arrangement of fuel rods within the storage cavity, with the objective of ascertaining the sensitivity of criticality safety to variations in pin pitch. The study will explore the impact of fuel rod arrangement on k_{eff} through three distinct methods of variation. The first method, termed Uniform Arrangement by Blocks, is predicated on the division of all fuel rods into two distinct regions. The second method, known as Layer-by-Layer Determination, involves segmenting the fuel rods into nine separate regions. The third method, referred to as Birdcage Deformation, draws inspiration from the deformation patterns observed in pressured water reactor (PWR) fuel assemblies that may result from a vertical drop impact, resembling the structural distortion of a birdcage. In addition to examining these methods, this paper will conduct a comparative analysis to identify the arrangement that yields the highest value of k_{eff}. The exploration of non-uniform arrangements is crucial, as it can encapsulate a range of fuel rod mispositioning incidents that may occur during transportation accidents. This comprehensive approach is essential for determining the precise level of uncertainty in criticality safety analysis

Section 2 of this paper will introduce the nuclear code and the computational model employed in the study. Section 3 will delve into determination of the optimal moderating pitch and the reactivity distribution, elucidating the reasons why a non-uniform arrangement of fuel rods can potentially increase k_{eff} more significantly than a uniform arrangement. Section 4 will proceed to examine the peak values of k_{eff} attainable through the application of non-uniform arrangement methods. It will also present a comparative analysis of the results yield by these methods, aiming to identify the most effective arrangement in terms of maximizing reactivity. Section 5 will extend the analytical methodology developed herein to a specific type of fuel assembly transport container, conducting a comparative analysis with the prevailing methods currently in use. Finally, this paper will culminate in a comprehensive summary of the findings presented throughout the paper.

2 Criticality code and computational model

2.1 Introduction of criticality code

The Monte Carlo particle transport program JMCT was employed for the computational aspects of this research endeavor [33]. The essential nuclear data utilized in these calculations were procured from the comprehensive nuclear database, ENDF/B-VI. In this paper, the Monte Carlo methodology was applied with a configuration that initiated each generation with 10,000 input neutrons. The simulation encompassed a total of 1,000 generations, with 800 of these generations designated as the active phase of the simulation. The computation of this research was conducted on our personal workstation, equipped with a Intel(R) Core(TM) i7-13700KF CPU and a NVIDIA GeForce RTX 3080 GPU. The computational effort required for a single computational document is estimated to be approximately 40 min.

The Monte Carlo approach is distinguished by its ability to provide a realistic portrayal of actual physical phenomena. To a significant extent, this methodology has the potential to supplement, and in some cases, supplant traditional physical experimentation. Consequently, it has emerged as an exceptionally potent instrument for addressing practical challenges within the realm of experimental nuclear physics [34].

However, American National Standards Institute/American Nuclear Society (ANSI/ANS) national standards 8.1 [35] and 8.24 [36] require that nuclear criticality safety analysts determine through validation what value of the k_{eff} predicted by software can be treated as subcritical, which means the computational method must be performed a validation study to determine its predictive capability for computing k_{eff} [37]. In the context of the transportation of PWR fuel assemblies, the storage systems are typically characterized by low enrichment and a specific rod-bundle design. In the event of the most extreme scenario involving water ingress, the system can be conceptualized as one where light water serves as the moderator. Consequently, the selection of pitch-type, low-enrichment uranium compound systems is deemed appropriate for establishing a criticality benchmark experiment. The reference [33] presents a computational analysis of the k_{eff} values for 107 such benchmark experiments. The findings indicate that the calculated k_{eff} values are in close proximity to their experimental counterparts. This congruence substantiates the assertion that the JMCT program possesses commendable computational precision when addressing problems of this nature.

2.2 Computational model

The computational models presented in this paper are predicated on a AFA3G-type fuel assembly and a specific type of spent fuel transport package. A schematic representation of the AFA3G-type fuel assembly is depicted in Fig. 1. The primary objective of this research is to assess the sensitivity of the effective multiplication factor, denoted as k_{eff}, to the arrangement of fuel rods. In an effort to conserve computational resources, the detailed structures of the transportation containers have been omitted from the model, with the focus

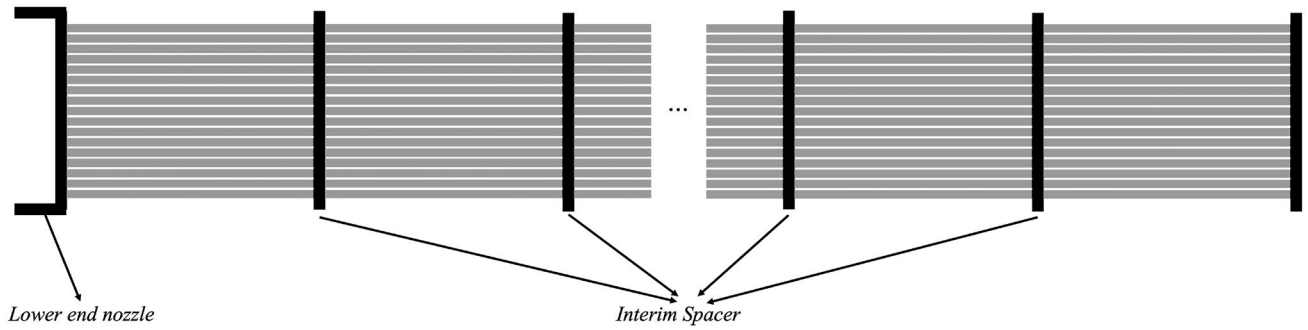

Fig. 1 Schematic diagram of AFA3G-type fuel assembly

being solely on the representation of a single fuel assembly. The Monte Carlo computational modeling of the fuel assemblies incorporates certain conservative assumptions that are grounded in the actual physical model. A comparative analysis of the principal characteristics between the basic computational model and the real-world model is presented in Table 1 The cross-sectional view of the basic computational model is illustrated in Fig. 3. These conservative assumptions, which are integral to the modeling process, are enumerated as follows:

a. The enrichment level of the computational model is set at 5 weight percent (wt%), which exceeds that of the fresh AFA3G-type fuel unit. This discrepancy is a deliberate choice to ensure a more conservative estimate of the fuel's reactivity.
b. This paper postulates a scenario where the fuel assembly is entirely submerged in water, which represents the most extreme condition conceivable. Under the auspices of conventional or standard transport protocols, this type of nuclear fuel assemblies are typically conveyed in a dry state. Nonetheless, in accordance with the stipulations of standard [5], a criticality safety analysis must encompass a comprehensive evaluation of potential unforeseen incidents that could jeopardize criticality safety, with particular emphasis on the possibility of water ingress. Such a condition could notably elevate k_{eff}, due to the moderating effect of water on neutrons, which could potentially lead to a higher probability of a sustained nuclear chain reaction [38].
c. This study assumes that the diameter of the gauge or guide tubes is equivalent to that of the fuel rods to facilitate the modeling of non-uniform arrangements of fuel rods. To ensure the conservatism of this assumption, the research conducted a sensitivity analysis on the impact of the gauge/guide tube diameter on k_{eff}. The findings indicate that this assumption leads to an increase in k_{eff} of 113 pcm, which confirms that the assumption is con-

Table 1 Real-world model vs. computational model

Main features	Real-world model	Computational model
Type of fuel assembly	17×17	17×17
Number of fuel rods	264	264
Fuel pallet diameter (mm)	8.192	8.192
Material of fuel pallet (wt%)	UO_2 4.5	UO_2 5
Fuel tube inner diameter (mm)	8.36	8.36
Fuel tube outer diameter (mm)	9.5	9.5
Number of guide tube	24	24
Number of gauge tube	1	1
Guide/gauge tube inner diameter (mm)	11.45	8.36
Guide/gauge tube outer diameter (mm)	12.45	9.5
Material of tube clad	M5 alloy	M5 alloy
Length of active zone (mm)	3657.6	3657.6
Nominal pin pitch (mm)	12.6	12.6
Inner size of storage tank (mm^2)	224.5×224.5	224.5×224.5
Material out of the tube	Air	Light water
Density of material out of the tube ($kg \cdot m^{-3}$)	1.29	1×10^3

servative, i.e., meaning that it errs on the side of caution by potentially overestimating the reactivity.

The difficulty of establishing the computational model is that the potential for fuel rod buckling following a transportation incident necessitates consideration of variations in pin pitch along the length of the fuel assembly. Drawing inspiration from the methodologies presented in Refs. [28, 31, 32], this paper simplifies the complex deformation of the fuel unit into a manageable single-variable problem. In alignment with these precedents, it is posited that the pin pitch undergoes uniform alteration across the entire active zone, thereby precluding the simulation of fuel tube buckling in the computational model. The outcomes of mechanical testing have elucidated that lattice expansion predominantly occurs in the regions adjacent to the collision [27]. Furthermore, the reactivity is contingent upon the extent of the lattice expansion zone; an elongation of this zone is directly correlated with an increase in reactivity [39]. This analytical approach is inherently conservative, as it accounts for the worst-case scenario without underestimating the potential for reactivity enhancement due to mechanical deformation.

The adoption of conservative manipulations in this research is of paramount importance, as it serves to encompass the uncertainties and potential variations that could potentially impact the safety of the system. By integrating a conservative approach into the study, the robustness of the results is enhanced, ensuring reliability even under the most stringent conditions. This methodological prudence is essential in maintaining the integrity of the system's safety margins and in providing a buffer against unforeseen circumstances that could arise during the transportation or operation of nuclear facilities.

3 Preliminary work

The primary objective of the research presented in this section is to ascertain the optimal strategy for the rearrangement of fuel rods.

3.1 Research of optimal moderating pin pitch for AFA3G-type fuel assembly

Light water reactor fuel assemblies are meticulously engineered with moderation in mind [12]. This implies that the neutrons released by the fissile material are not sufficiently moderated at their nominal pitch. Increasing the pin pitch results in an enhanced water–uranium ratio, which in turn allows for a greater proportion of neutrons to be fully moderated before engaging with the fuel. Consequently, the reactivity of the fuel assembly escalates. It is important to note that beyond the optimal pitch, a further expansion of the pitch will lead to a decline in reactivity, as a significant portion of the neutrons is absorbed by water.

In this study, an infinite array of fuel rods was modeled to investigate the impact of pitch on reactivity. k_{eff} was calculated of these systems at various pitches. The objective was to delineate the relationship between fuel rod pitch and reactivity. The pitch was varied from the standard value of 0.0126 m to the average neuron migration length in light water, which is 0.028 m [40]. The analysis revealed that k_{eff} initially increases with the increase in pin pitch, reaching a peak before declining, as illustrated in Fig. 2. This phenomenon is consistent with our conjecture. The peak of this curve signifies the optimal moderated pitch for AFA3G-type fuel unit, determined to be (0.0154 ± 0.0002) m.

In the scenario where fuel rods uniformly occupy the entire storage tank, the pitch is determined to be about 0.0134 m, a value that falls short of the optimal moderating pitch. A report by CNPRI suggests that selectively compressing a subset of the fuel rod pitches to expand others can enhance k_{eff} further, given the condition of the fuel rods uniformly filling the storage tank. The current inquiry pertains to the strategic selection of which section of the fuel rod pitch to expand for maximum reactivity improvement.

3.2 Reactivity distribution

Employing a track length estimator facilitates the determination of the reactivity distribution across the radial extent of a fuel assembly [32]. Leveraging the inherent symmetry of fuel assemblies, this study modeled only a quarter of the assembly when examining the reactivity distribution, specifically for a AFA3G-type fuel assembly. The selected portion for modeling, depicted within the red boundary in Fig. 3, encompasses a 9×9 rods. The boundaries delineated by the left and lower edges of red box in Fig. 3 exhibit the surfaces

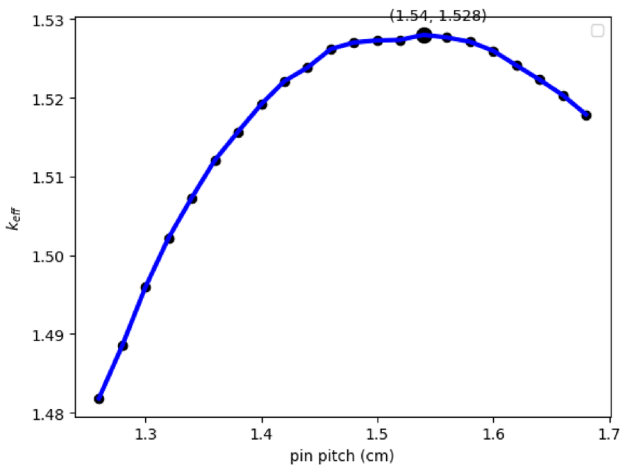

Fig. 2 (Color online) Study of optimal moderate pitch

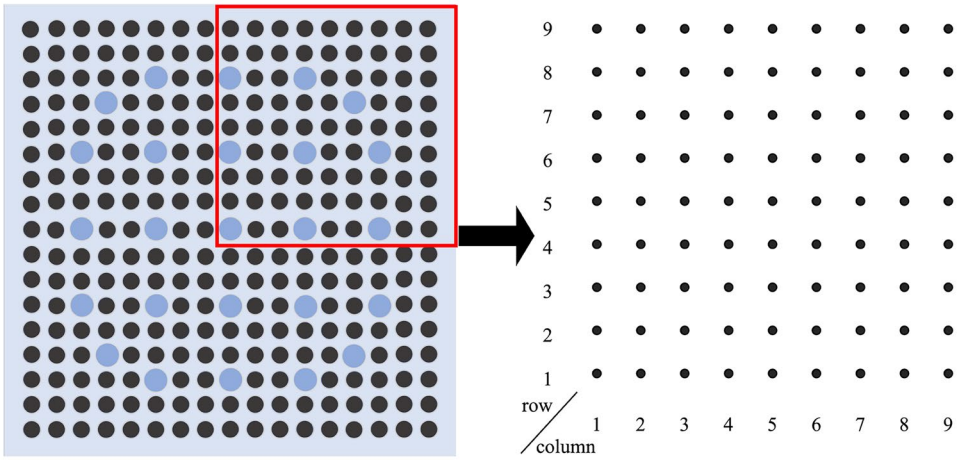

Fig. 3 (Color online) Illustration of computational model

of total internal reflection, whereas the remaining boundaries are devoid of any reflective properties.

Let $r_{i,j}$ denote the reactivity of the fuel rod located in the i-th row and j-th column. For the guide or gauge tube situated in the j-th row, a direct calculation using the Monte Carlo code was not employed. Consequently, the reactivity located at gauge or guide tubes are estimated by taking the average reactivity of the fuel rods that are positioned immediately above and below the guide tube. The reactivity $r_{i,j}$ for the guide tube can be derived from Eq. (1):

$$r_{i,j} = \begin{cases} \frac{r_{i-1,j}+r_{i+1,j}+r_{i,j-1}+r_{i,j+1}}{4} & i,j > 1 \\ \frac{2r_{i+1,j}+r_{i,j-1}+r_{i,j+1}}{4} & i = 1, j > 1 \\ \frac{r_{i-1,j}+r_{i+1,j}+2r_{i,j+1}}{4} & i > 1, j = 1 \\ \frac{r_{i+1,j}+r_{i,j+1}}{2} & i = 1, j = 1 \end{cases} \tag{1}$$

The analysis results in a 9×9 matrix where each entry corresponds to the reactivity of the respective fuel rod. From this matrix, one can construct the weighted average reactivity distribution matrix, denoted as $\mathbf{R}^{9\times9}$. The formula for calculating each element of this matrix is presented in Eq. (2).

$$\hat{r}_{i,j} = \frac{r_{i,j}}{\sum_{i=1}^{9}\sum_{j=1}^{9} r_{i,j}} \tag{2}$$

Figure 4 illustrates the reactivity distribution following the weighted averaging of a quarter of the fuel assembly. The lower left square within Fig. 4 denotes the central fuel rod of a fuel subassembly. An observation made from Fig. 4 is that the reactivity of a fuel rod increases as it approaches the center of the assembly. Consequently, it can be inferred that the fuel rods in the central region have a more significant impact on the overall reactivity.

In summary, the non-uniform distribution of fuel rods, especially the strategic enlargement of the pitch in the central region to approximate the optimal moderating pitch,

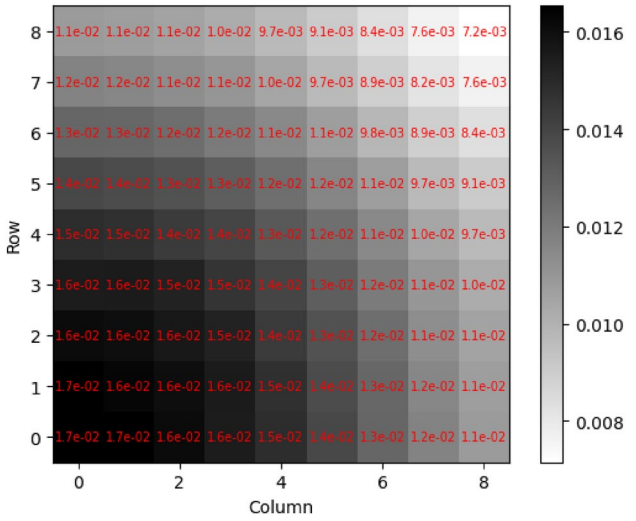

Fig. 4 (Color online) Reactivity distribution in 1/4 AFA3G-type fuel assembly

presents a considerable potential to markedly elevate k_{eff}. Nonetheless, given the extensive array of possible configurations for fuel rod arrangement, a systematic and methodical approach is imperative for identifying the configuration that yields the highest reactivity.

4 Non-uniform arrangement methodology

As established in Sect. 3.B, the reactivity within a fuel unit is distributed in an inhomogeneous manner. In this section, this paper explore the rearrangement of fuel rods using three distinct non-uniform configuration strategies, each aimed at maximizing k_{eff}. The first strategy is termed Uniform Arrangement by Blocks, the second is known as Layer-by-layer Determination, and the third is referred to as Birdcage Deformation. The input files for the various computational

examples in this section are all generated using a custom Python script.

4.1 Uniform arrangement by blocks

The initial non-uniform method discussed in this paper is designated as Uniform Arrangement by Blocks. This nomenclature stems from the characteristic that, while the pin pitches may vary across different regions, they remain consistent within a single region. In this approach, the fuel rods completely occupy the storage tank, and an expansion of the pitch in the central area curtails a corresponding adjustment in the pitch of the peripheral regions. The core principle of this method involves segmenting a fuel subassembly into two distinct regions by rods: the central region and the surrounding region.

The delineation of the central region is contingent upon the number of fuel rods, ensuring an equal count in each row and column. The count of fuel rods in any given row or column of central region is an odd number, ranging from 3 to 15. It is imperative to recognize that the central region maintains a square cross section, with its Fermat point aligning with that of the storage tank's cross section. The division of the central region into distinct configurations is variable, offering seven distinct options that scale from a 3×3 to a 15×15 arrangement of fuel rods. These various division methods are graphically represented in Fig. 5.

Among the various methods of division, the pitch within the central region is incrementally increased from the nominal value until it reaches the location where the surrounding fuel rods are at a contact pitch. The mathematical relationship between the pitch of the short side of the surrounding fuel rods and the pitch in the central region can be derived and is presented in Eq. (3).

$$p_s = \frac{8D - n_c p_c}{8 - n_c} \tag{3}$$

In this context, D is the nominal pin pitch, p_s denotes the length of the short side of the pitch surrounding the fuel rods, while p_c signifies the pitch of the fuel rods in the central area. Additionally, n_c is used to represent the number of pitches between each row or column within the central region. This configuration is visually depicted in Fig. 6, which serves to illustrate the geometric relationships and parameters involved in the Eq. (3).

The input files for these calculations incorporate a parameter known as the expansion coefficient, denoted by ε, which is utilized to quantify the expand degree of the central region. Within a given division method, a lower value of ε corresponds to a smaller pitch in the central area, whereas a higher value of ε signifies a more expansive central region. ε is defined by the ratio of the cross-sectional surface of the central region to that of the entire storage tank. The mathematical formulation for ε is detailed in Eq. (4).

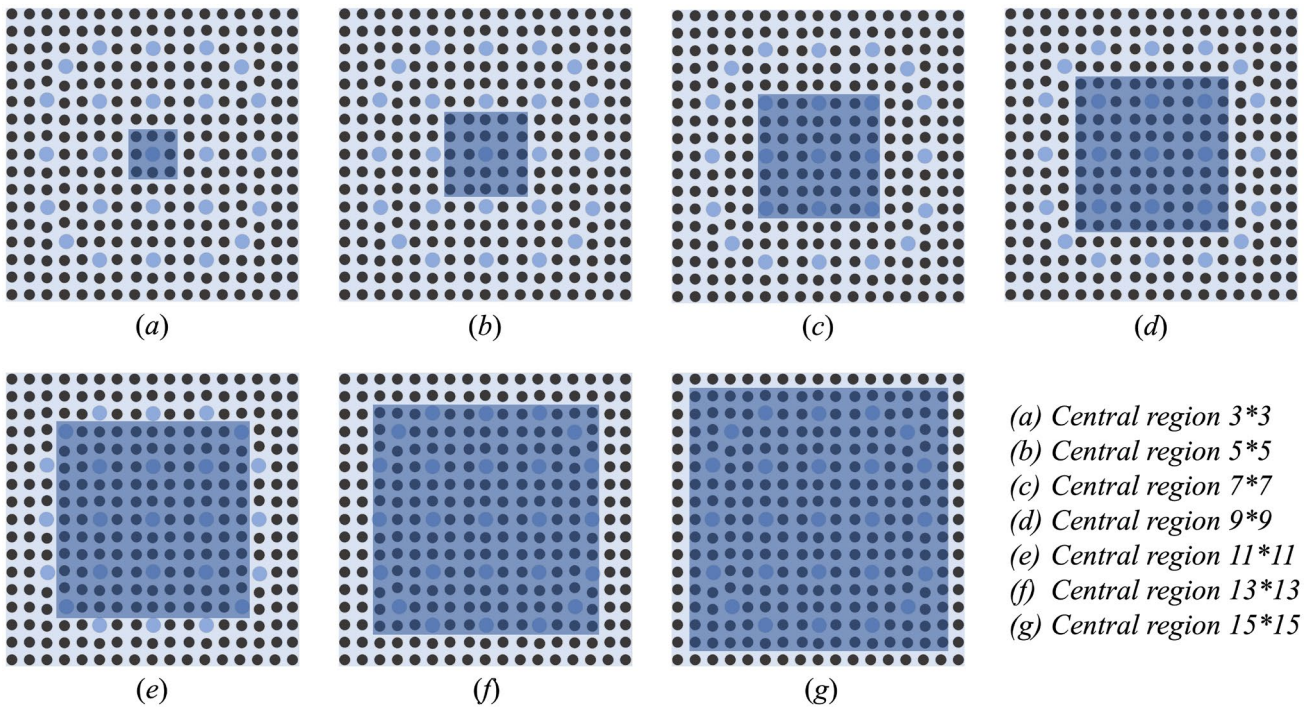

Fig. 5 (Color online) Seven ways to divide a fuel assembly

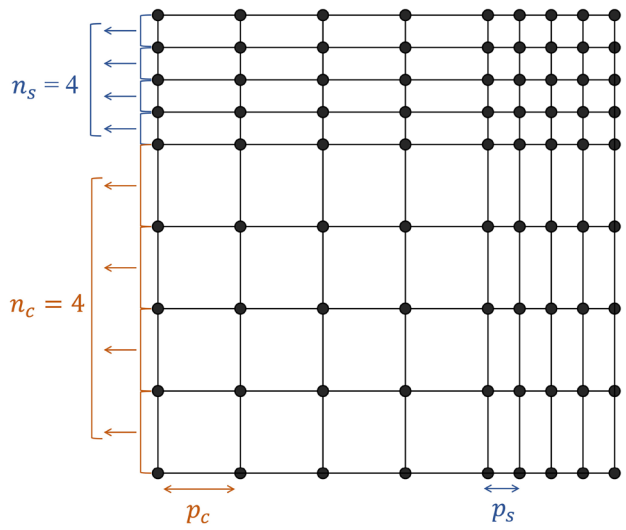

Fig. 6 Illustration of Eq. 3, where $n_s = n_c = 4$

$$\varepsilon = \frac{S_c}{S_n} = \frac{n_c^2 p_c^2}{64D^2} \tag{4}$$

In the given formulation, S_c symbolizes the cross-sectional surface of the central region, and S_n denotes the cross-sectional surface of the storage cavity. The terms n_c, p_c and D used here retain the same meanings as previously defined in the text.

Figure 7 demonstrates the trends of k_{eff} changing with the ε for each division approach. The peak value of k_{eff} is observed when the central region is configured as a 13×13 grid, with the fuel rods in this region being fully expanded. Under these conditions, the pitch in the central region is measured at 0.01475 m, and k_{eff} reaches a value of 0.99793. The specific arrangement is depicted in Fig. 17a, while the positions of each fuel rod along the central axis are detailed in Table 4.

4.2 Layer-by-layer determination

The method discussed in this section is a non-uniform arrangement technique introduced in Ref. [31]. It offers a more nuanced partitioning of the fuel subassembly compared to the Uniform Arrangement by Blocks. While the latter approach simply divides the fuel element into two distinct region by rods, the method under consideration further subdivides the fuel assembly into nine distinct zones by layer, as illustrated in Fig. 8. However, it is anticipated that this more complex partitioning may result in an arrangement with higher reactivity when compared to the Uniform Arrangement by Blocks.

Figure 9 provides a visual representation of this method, with a detailed explanation presented subsequently:

a. Initially, uniformly increase the pitch of all fuel rods until the 9-th layer reaches contact with the inner surface of the storage tank. By plotting the curve of k_{eff} against pitch, identify the configuration of fuel rods that corresponds to the maximum k_{eff}. Retain the position of the 9-th layer as determined.
b. Subsequently, uniformly increase the pitch for the remaining layers of fuel rods, until the 8-th layer's rods are in contact with those of the 9-th. Plot the curve of k_{eff} against pitch to ascertain the arrangement of fuel rods that yields the maximum k_{eff}. Maintain the configuration of the 8-th layer as such.
c. Progressively reduce the number of fuel rods subject to variation and iteratively apply the process from step b. Determine the positions of fuel rods from the outer layer to the inner layer, continuing this process until the

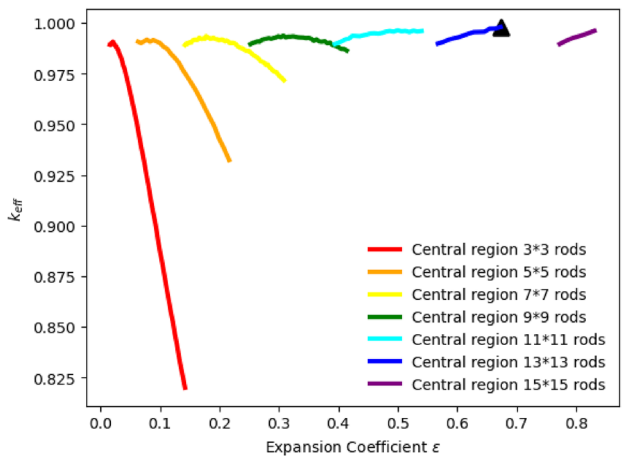

Fig. 7 (Color online) Result of uniform arrangement by blocks

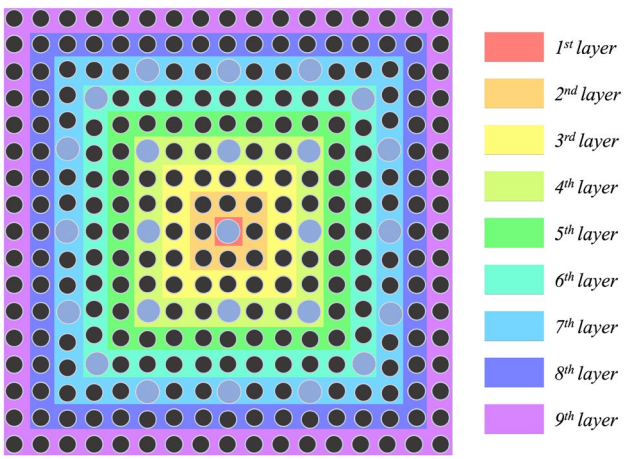

Fig. 8 (Color online) Division a fuel assembly by layers

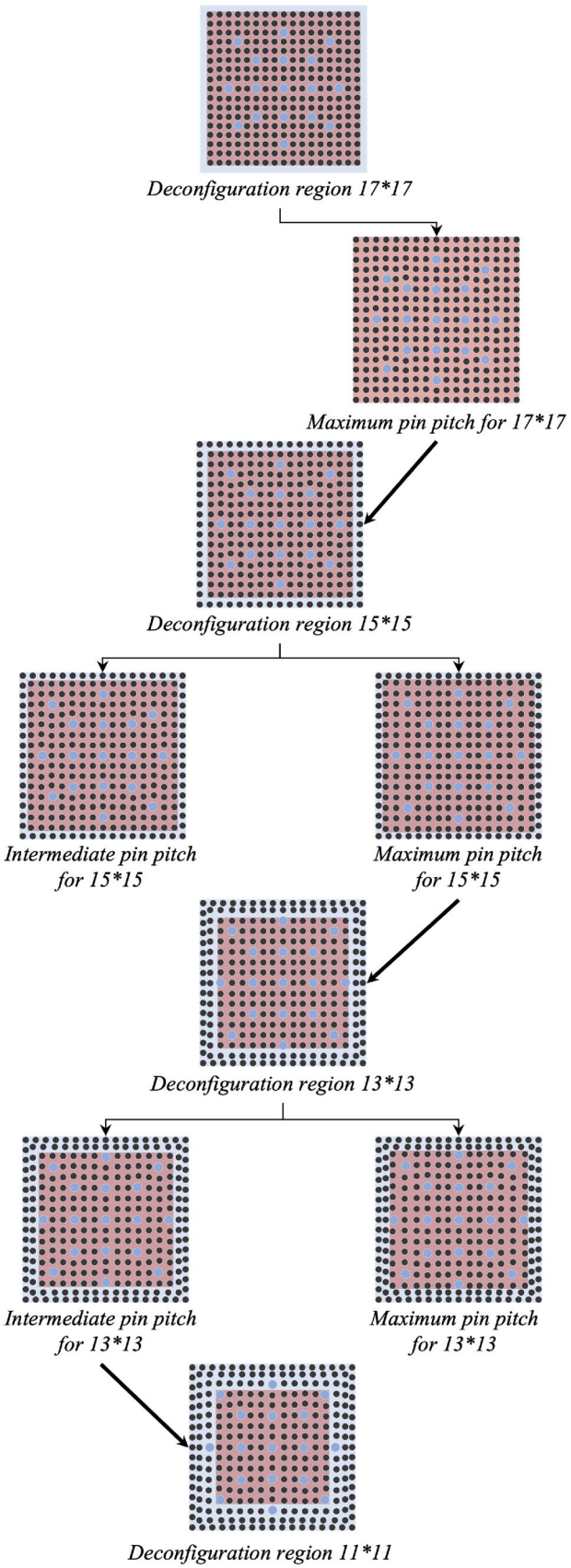

Fig. 9 (Color online) Process of determination layer-by-layer

changes in arrangement no longer results in an increase in k_{eff}.

The positions of the fuel rods were determined through the systematic procedures previously outlined. Figure 10a illustrates the variation of k_{eff} with the uniform increase in pitch of all fuel rods, which was instrumental in establishing the locations of the outermost layer of rods. Figure 10b depicts the change in k_{eff} with the pitch increase of the remaining 225 rods, thereby determining the positions of the 8-th layer of rods. The pitch between the 8-th and 9-th layer fuel rods, identified as the contact pitch, is 0.0095 m, as derived from Fig. 10b. Figure 10c shows the k_{eff} variation with the pitch increase of the remaining 169 rods, which was used to ascertain the positions of the 7-th layer of rods. The pitch from the 7-th to the 8-th layer fuel rods is 0.0104 m, as extracted from Fig. 10c. Additionally, Fig. 10d indicates a pitch of 0.0126 m between the 6-th and 7-th layer fuel rods. In Fig. 10c and d, noticeable fluctuations in k_{eff} values are observed, attributed to the inherent statistical variability of the Monte Carlo calculation method. These fluctuations suggest that as the arrangement of fuel rods approaches the configuration that maximizes k_{eff}, the impact of the rod arrangement on k_{eff} diminishes, the statistical fluctuations inherent in the program itself are more pronounced. Subsequently, the pitch of the remaining five inner layers of fuel rods was uniformly increased. It was observed that k_{eff} decreases with increasing pitch, as shown in Fig. 11. Consequently, a uniform pitch of 0.015 m was adopted between the remaining layers of fuel rods.

The upper limit of k_{eff} attainable through this variation method is 0.99827. This optimal arrangement is depicted in Fig. 17b, with the specific location of each fuel rod along the central axis detailed in Table 4. The maximum value of k_{eff} achieved by employing this method surpasses that obtained by the Uniform Arrangement by Blocks technique.

4.3 Birdcage deformation

The mechanical tests referenced in [23, 24] indicate that the most adverse scenario for a fuel assembly is when it experiences a vertical drop. In such an event, the deformation of the lower nozzle has the potential to cause significant damage at the impact end of the fuel rods [41]. The tests demonstrate that for PWR fuel assemblies, a specific type of deformation known as 'Birdcage Deformation' typically occurs in the region between the lower nozzle and the first interim spacer. This phenomenon is illustrated in Fig. 12.

The methodology presented in paper [32] delineates a three-step process for ascertaining the positions of fuel rods, as depicted in Fig. 13. Initially, the location of the outermost layer of fuel rods is established. Subsequently, the positions of the fuel rods along the axis of symmetry

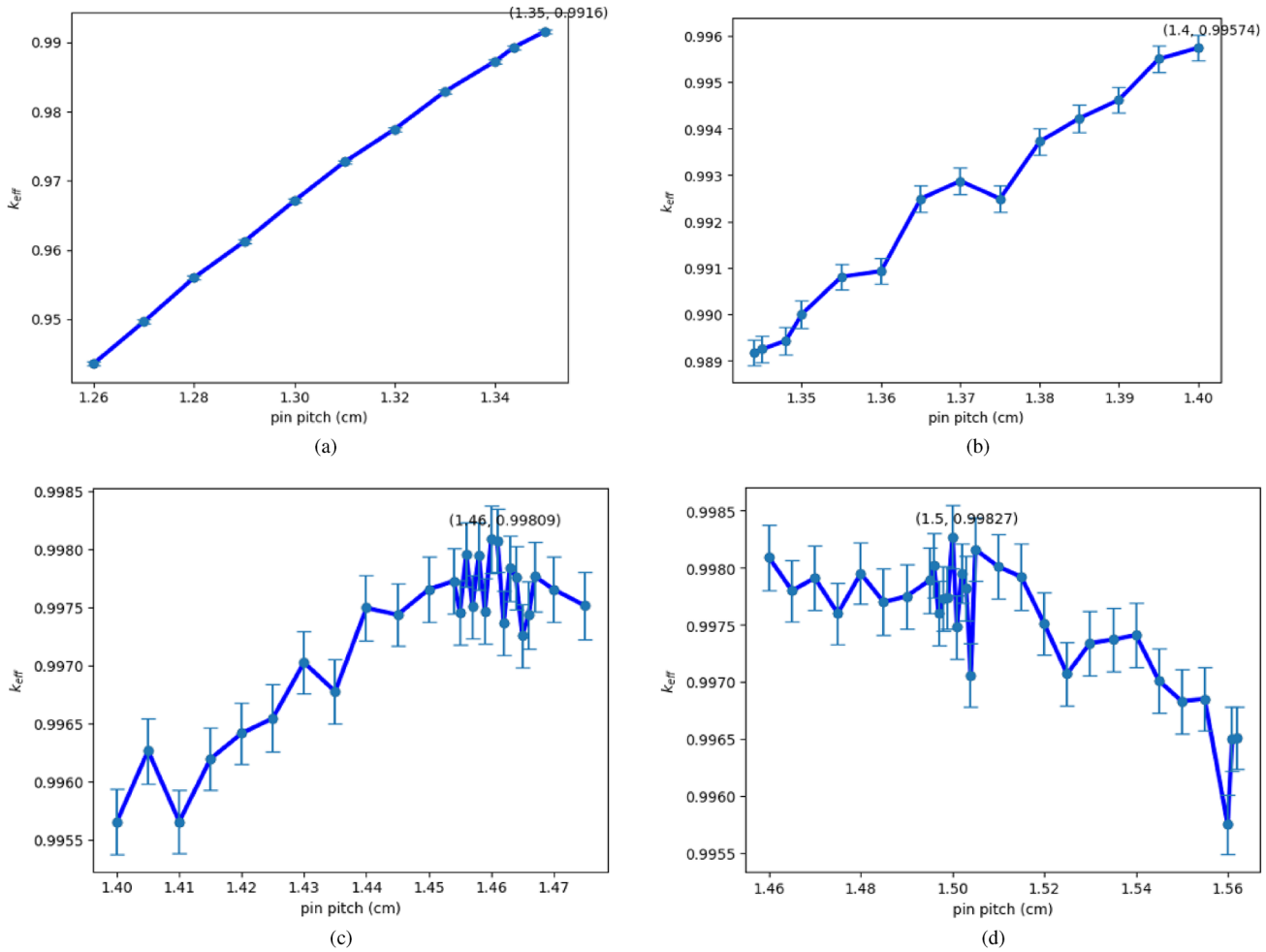

Fig. 10 (Color online) Determining rods' location layer by layer. **a** Determining 9-th layer fuel rods. **b** Determining 8-th layer fuel rods. **c** Determining 7-th layer fuel rods. **d** Determining 6-th layer fuel rods

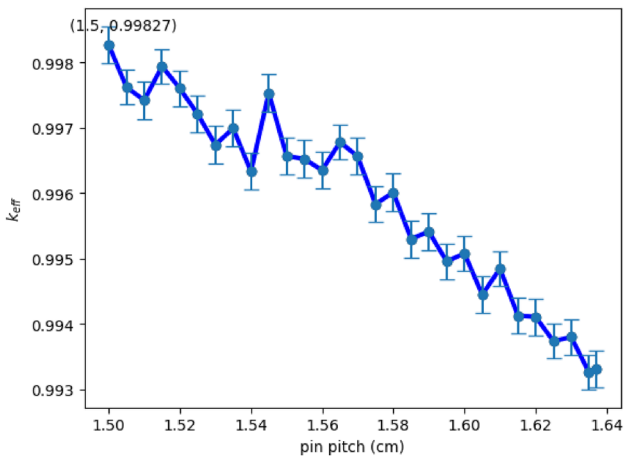

Fig. 11 (Color online) Effect of uniform variation of five layers of rods on k_{eff}

are determined. Lastly, the locations of the remaining fuel rods are ascertained. It is presumed that the outer rows of pins are uniformly aligned against the basket wall. The positions of the remaining fuel rods are derived through the application of natural boundary condition cubic spline interpolation. This paper builds upon this concept, but introduces revisions to the mathematical model used for determining the positions of the fuel rods along the symmetric axis.

The present study introduces revisions to the existing mathematical model, which was found to be inadequate in accurately capturing the true nature of Birdcage Deformation. Drawing from the design specifications for PWR fuel subassemblies, the lower ends of the fuel rods are not affixed to the lower nozzle, implying that they are free to move relative to one another. This is in contrast to the older method, which assumed that the fuel rods were immobile in relation to each other. Consequently, the revised mathematical model offers a more realistic representation of the actual conditions

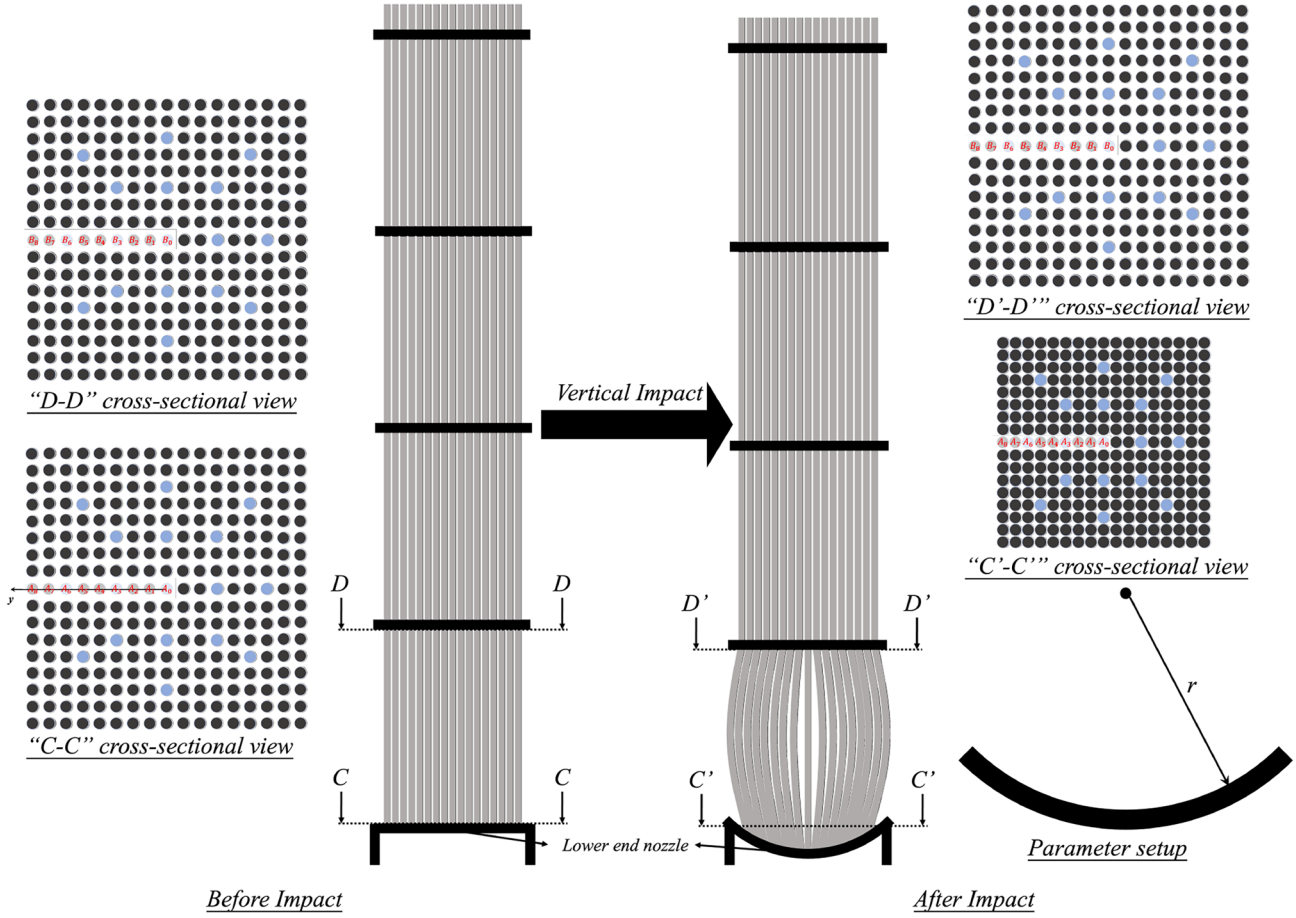

Fig. 12 Illustration of Birdcage Deformation

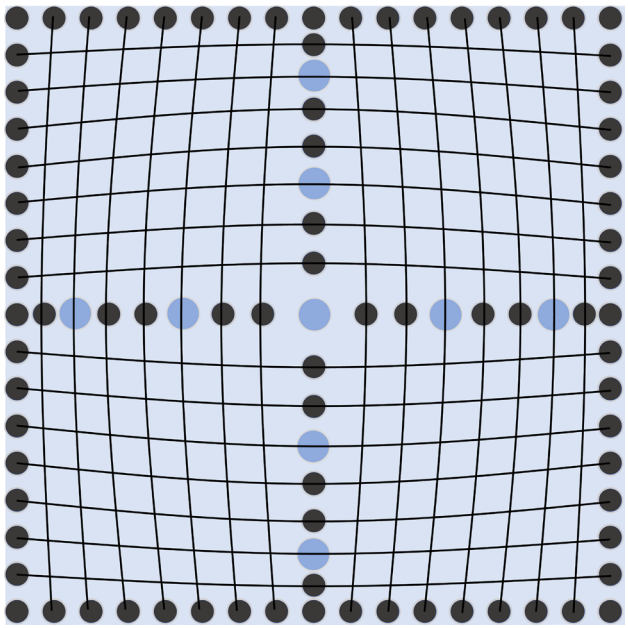

Fig. 13 Steps of Birdcage Deformation to determine fuel rods' location

encountered in PWR fuel assemblies. The following sections will elaborate on this novel approach in detail.

Figure 14 provides a visual representation of the revised mathematical model. Within Fig. 14, the dotted arc on the left represents the lower nozzle, and the vertical dotted line on the right represents the first fuel element interim spacer. A_0B_0 represents the centermost fuel rod, and A_1B_1 to A_8B_8 represent the remaining eight fuel rods on the half of a symmetric axis. d is contact pitch, while D represents nominal pitch. Assuming when the Birdcage Deformation occurs, the following conditions are considered:

a. The lower nozzle undergoes deformation such that it becomes part of a spherical surface with a radius of curvature r.
b. The impacted ends of the fuel rods come into contact with one another, while the fuel rods at the first interim spacer maintain their nominal pitch.
c. The central fuel rod is assumed to remain straight, while the peripheral fuel rods are modeled to exhibit curvature. The arc length of the bends in these fuel rods is equiv-

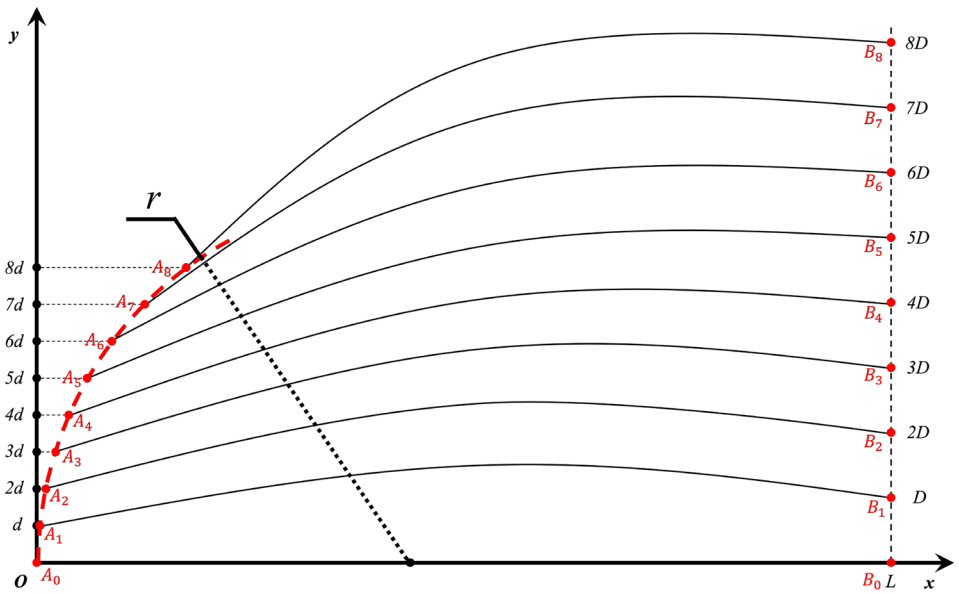

Fig. 14 Mathematical model of new Birdcage Deformation

alent to the nominal distance to the nominal distance between the lower nozzle and the first interim spacer.

These assumptions ensure that the model accurately reflects the Birdcage Deformation characteristics of the fuel rods under the vertical drop accident.

Within the framework of this mathematical model, the deformation of the lower nozzle is represented as a circular arc when projected onto the *xoy* plane in Fig. 14. Let A_i denote the lower end of i-th fuel rod. The horizontal coordinate of A_i in Fig. 14 is represented by x_{A_i}. The value of x_{A_i} can be mathematically expressed in Eq. (5):

$$x_{A_i} = r - \sqrt{r^2 - (id)^2} \tag{5}$$

where r signifies the radius of curvature of the deformed lower nozzle, and d denotes the diameter of the fuel rod. Utilizing these parameters, the horizontal coordinate x_{A_i} for the lower end of the i-th fuel rod, where i ranges from 1 to 8, can be determined. The coordinates of the lower end of these fuel rods, specifically A_1 through A_8, are derived and expressed in the form $(x_{A_i},\ id)$.

Let L be the nominal distance between the lower nozzle and the first interim spacer. The term θ_i signifies the angular position of the center of the circular arc that corresponds to the deformation of the i-th fuel rod. This angle is a key parameter in the geometric description of the rod's configuration following the deformation process. Finally, the variable R_i is designated to represent the radius of curvature of i-th fuel rod. According to the geometric relationship, the interrelation among the above parameters, including L, θ_i, R_i and x_{A_i}, can be mathematically expressed by Eq. (6):

$$\begin{cases} \frac{L}{2\pi R_i} = \frac{\theta_i}{2\pi} \\ \sin\frac{\theta_i}{2} = \frac{\sqrt{(L-x_{A_i})^2 + i^2(D-d)^2}}{2R_i} \end{cases} \tag{6}$$

where D denotes the nominal pin pitch, defining the standard distance between the centers of adjacent fuel rods. The symbol d signifies the contact pin pitch, representing rods are in contact due to deformation. The variable i iterates over the set $\{1, 2, 3, \cdots, 8\}$, corresponding to each individual fuel rods being considered in the model. Upon organizing Eq. (6), a more streamlined formulation, Eq. (7), can be derived. This reorganization elucidates the interrelationships among the parameters, potentially enhancing the ease of further analysis and computational applications.

$$\sin\frac{L}{2R_i} = \frac{L}{2R_i}\sqrt{(1 - x_{A_i}/L)^2 + i^2(D/L - d/L)^2} \tag{7}$$

Then, introducing the variable t_i, expressed as $t_i = \frac{L}{2R_i}$. Additionally, defining M_i, expressed as $M_i = \sqrt{(1 - x_{A_i}/L)^2 + i^2(D/L - d/L)^2}$. Utilizing these definitions, Eq. (7) can be succinctly re-expressed in a simpler form as presented in Eq. (8).

$$\sin t_i = M_i t_i, \quad t_i \in (0, +\infty) \tag{8}$$

Given that x_{A_i}, D, and d are significantly smaller than L, the value of M_i is approximately equal to 1, albeit slightly less. Considering the growth rates of the functions $f(x) = \sin(x)$ and $f(x) = x$, it can be deduced that Eq. (8) possesses a unique root within its domain of definition, which is marginally greater than zero. By solving Eq. (8), the value of t_i can be determined, and subsequently, R_i can be calculated.

The coordinate of point B_i are specified as (L, iD). Accordingly, the midpoint of the line segment A_iB_i is located at the coordinates $\left(\frac{L+x_{A_i}}{2}, \frac{i(D+d)}{2}\right)$. Given these coordinates, the slope k_i of line containing the segment A_iB_i is $k_i = \frac{i(D-d)}{L-x_{A_i}}$. Employing this slope, the equation of the perpendicular bisector of the line segment A_iB_i is formulated and provided in Eq. (9). The letters within the formula maintain the same significance as previously defined in the discussion.

$$y_i = -\frac{L - x_{A_i}}{i(D-d)}x_i + \frac{i(D+d)}{2} + \frac{L^2 - x_{A_i}^2}{2i(D-d)} \tag{9}$$

Let O_i denote the center of the circular arc $\overset{\frown}{A_iB_i}$, with coordinates (x_{O_i}, y_{O_i}). O_i lies on the perpendicular bisector of A_iB_i, and considering that the distance from O_i to B_i is equal to the radius of curvature R_i, the coordinates (x_{O_i}, y_{O_i}) can be determined by solving the system of equations presented in Eq. 10. The variables used within this formula adhere to the same definitions previously established in our discussion.

$$\begin{cases} (x_{O_i}^2 - L)^2 + (y_{O_i} - iD)^2 = R_i^2 \\ y_{O_i} = -\frac{L-x_{A_i}}{i(D-d)}x_{O_i} + \frac{i(D+d)}{2} + \frac{L^2-x_{A_i}^2}{2i(D-d)} \end{cases} \tag{10}$$

Equipped with the determined value of R_i and the precise coordinates of O_i, the geometric representation of the circular arc $\overset{\frown}{A_iB_i}$ is articulated in Eq. (11). This equation encapsulates the mathematical description of the arc, grounded in the established parameters and consistent with the previously defined variables.

$$y = y_{O_i} + \sqrt{R_i^2 - (x - x_{O_i})^2}, \quad x \in [x_{A_i}, L] \tag{11}$$

Consequently, the maximum radial distance of each rod $y_{\mathrm{i,max}}$ from the centermost rod is captured by the formulation presented in Eq. (12). This equation provides a quantitative measure of the spatial distribution of the rods relative to the central axis of the fuel assembly.

$$y_{\mathrm{i,max}} = y_{O_i} + R_i \tag{12}$$

With the mathematical model now established, the subsequent task is to delineate the range of variation for r and to establish the constraint that arise from the size of fuel assembly and storage tank. Upon examination of the parameters specific to the AFA3G-type fuel assembly, the values for d, D, and L are identified as 0.0095 m, 0.126 m, and 0.7015 m, respectively. This paper proceeds to determine the range of variation for r and the associated constraint conditions as detailed in the following sections.

a. Determination of the range for the variable r

In the context of this mathematical model, a smaller value of r signifies a more severe deformation of the lower nozzle. However, practical considerations dictate that the nozzle will not undergo a curling deformation under any plausible accidental conditions. Therefore, the minimum allowable radius of curvature, denoted as r_{min}, is constrained by the physical limitations of the nozzle and geometry. This minimum value is established through the formulation presented in Eq. (13):

$$r_{\mathrm{min}} = \frac{X - d}{\pi} \approx 0.0685\ \mathrm{m}, \tag{13}$$

where X represents the side length of the storage cavity, and X is 0.2245 m. As the value of r increases, the deformation of the lower nozzle becomes progressively milder. However, this mathematical model is predicated on the assumption that the lower ends of the fuel rod remain in contact with one another. To ensure that the fuel rods within the model do not separate or become disengaged, the maximum value of r must be such that the fuel rod represented by A_8B_8 remains unbent. Under this condition, the maximum radius of curvature, denoted as r_{max}, is determined and can be articulated by Eq. (14):

$$r_{\mathrm{max}} = L - \sqrt{L^2 - 8^2(D-d)^2} \approx 6.58\ \mathrm{m} \tag{14}$$

The determination of r_{max} is also governed by the condition that the location corresponding to the maximum pitch must fall within the span between the lower nozzle and the first interim spacer. Consequently, any value of x_{O_i} exceeding L is not representative of the scenario modeled by this mathematical framework. To explore this boundary condition, a Python program was coded as port of this research to calculate the value of r when x_{O_i} equals L, yielding $r = 4.94$ m.

Taking into account both the minimum and maximum conditions described above, the radius of curvature r in this mathematical model is constrained to vary within the range of 0.07 m to 4.94 m.

b. Determination the constraint condition

Table 2 Limit of y_{max} of each layer of fuel rods. (The definition of layer is consistent with that illustrated in Fig. 8)

Layer	y_{max} (m)
1	0
2	0.041
3	0.0505
4	0.06
5	0.0695
6	0.079
7	0.0885
8	0.098
9	0.1075

Constraint conditions are essential as they define the permissible bounds within which the model operates, ensuring that the mathematical representation aligns with physical realities and practical limitations. These conditions are derived from a comprehensive consideration of the system's geometry and operational parameters.

Given that the fuel assembly must remain within the confines of the storage cavity under all conditions, including potential accident scenarios, each fuel rod is subject to its own boundaries of motion. These boundaries are crucial for establishing the constraints within the mathematical model and are detailed in Table 2, which outlines the permissible limits of movement for the fuel rods.

Utilizing former Python program, the positions of the fuel rods were calculated for a range of radii r extending from 0.07 m to 4.94 m. The corresponding maximum y-values,

Table 3 Values for y_{max} varying with r. (The definition of layer is consistent with that illustrated in Fig. 8)

	r (m)		
Layer	0.07	0.08	0.09
1	0	0	0
2	2.40451×10^{-2}	2.32032×10^{-2}	2.25057×10^{-2}
3	4.80648×10^{-2}	4.63856×10^{-2}	4.49938×10^{-2}
4	6.00000×10^{-2}	6.00000×10^{-2}	6.00000×10^{-2}
5	6.95000×10^{-2}	6.95000×10^{-2}	6.95000×10^{-2}
6	7.90000×10^{-2}	7.90000×10^{-2}	7.90000×10^{-2}
7	8.85000×10^{-2}	8.85000×10^{-2}	8.85000×10^{-2}
8	9.80000×10^{-2}	9.80000×10^{-2}	9.80000×10^{-2}
9	1.07500×10^{-1}	1.07500×10^{-1}	1.07500×10^{-1}
		...	
	r (m)		
Layer	1.90	1.91	1.92
1	0	0	0
2	1.34433×10^{-2}	1.34366×10^{-2}	1.34234×10^{-2}
3	2.68865×10^{-2}	2.68730×10^{-2}	2.68465×10^{-2}
4	4.03292×10^{-2}	4.03090×10^{-2}	4.02692×10^{-2}
5	5.37713×10^{-2}	5.37444×10^{-2}	5.36914×10^{-2}
6	6.72125×10^{-2}	6.71790×10^{-2}	6.71126×10^{-2}
7	8.06527×10^{-2}	8.06125×10^{-2}	8.05329×10^{-2}
8	9.40916×10^{-2}	9.40447×10^{-2}	9.39520×10^{-2}
9	1.07500×10^{-1}	1.07476×10^{-1}	1.07370×10^{-1}
		...	
	r (m)		
Layer	4.92	4.93	4.94
1	0	0	0
2	1.26001×10^{-2}	1.26000×10^{-2}	1.26000×10^{-2}
3	2.52001×10^{-2}	2.52000×10^{-2}	2.52000×10^{-2}
4	3.78002×10^{-2}	3.78000×10^{-2}	3.78000×10^{-2}
5	5.04002×10^{-2}	5.04001×10^{-2}	5.04000×10^{-2}
6	6.30003×10^{-2}	6.30001×10^{-2}	6.30000×10^{-2}
7	7.56003×10^{-2}	7.56001×10^{-2}	7.56000×10^{-2}
8	8.82003×10^{-2}	8.82001×10^{-2}	8.82000×10^{-2}
9	1.00803×10^{-1}	1.00801×10^{-1}	1.00800×10^{-1}

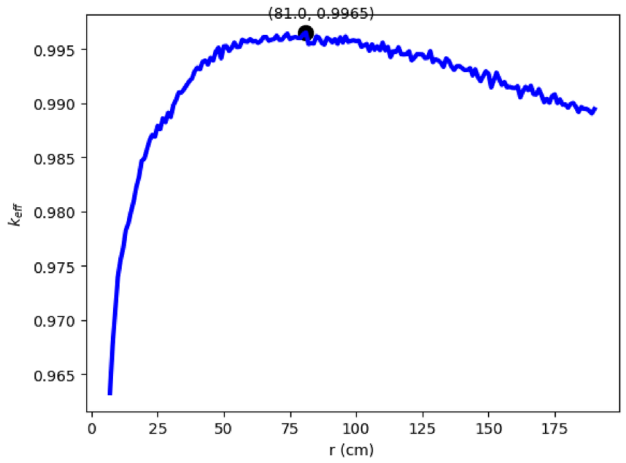

Fig. 15 (Color online) Effect of r on k_{eff}

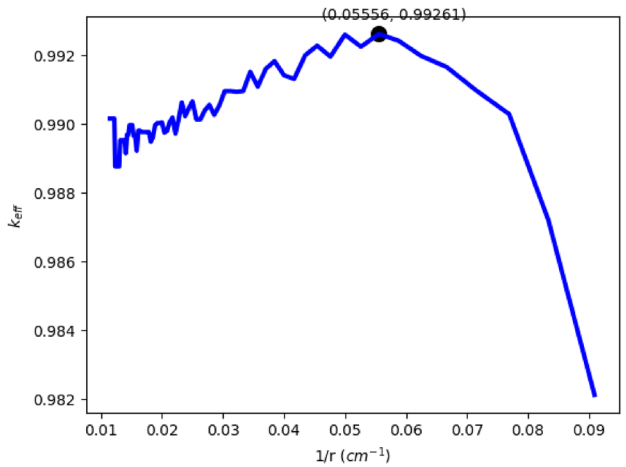

Fig. 16 (Color online) Effect of $1/r$ on k_{eff}

denoted as $y_{\max}$, are presented in Table 3. Analysis of the data in Table 3 reveals that when r exceeds 1.90 m, the rods are no longer able to fully occupy the storage tank. Consequently, in such instances, k_{eff} is anticipated to be lower than that in scenarios where the fuel rods can full fill the storage cavity.

The computational analysis has identified the maximum value of k_{eff} as occurring at $r = 0.81$ m, with k_{eff} reaching 0.9965, as shown in Fig. 15. This condition is characterized by a specific arrangement of the fuel rods, which is illustrated in Fig. 17(c). Furthermore, the configuration of the rods along the symmetric axis for this scenario is detailed in Table 4, providing a comprehensive view of the fuel assembly's geometry at the point of peak reactivity (Fig. 15).

This paper calculated the older Birdcage Deformation model proposed in Ref. [32] as well, and obtained the curve of k_{eff} versus r, see Fig. 16. The maximum value of k_{eff} occurs at $r = 0.18$ m, which is 0.99261. In this case, the fuel rod arrangement is shown in Fig. 17d, and the arrangement of fuel rods on the symmetric axis is shown in Table 4. The upper limit of the old mathematical model is smaller than that of the new birdcage mathematical model. In addition to the development of the new mathematical model, this paper also recalculated the older Birdcage Deformation model as initially proposed in Ref. [32]. The results of this calculation are presented in the form of a curve depicting the relationship between the k_{eff} and the radius of curvature r, as shown in Fig. 16. The maximum value of k_{eff} within the context of the old model was found to occur at $r = 0.18$ m, with k_{eff} peaking at 0.99261. The corresponding arrangement of the fuel rods for this scenario is illustrated in Fig. 17d, and the detailed layout of the fuel rods along the symmetric axis is provided in Table 4.

Upon comparison, it is observed that the upper limit of k_{eff} achieved by the old mathematical model is lower than that of the newly developed birdcage mathematical model. In conclusion, the New Birdcage Deformation demonstrates superior conservative capabilities and aligns more closely with realistic deformation scenarios compared to the model previous proposed in Ref. [10]. It is recommended that New Birdcage Deformation be considered over the Old Birdcage Deformation during criticality safety analysis. The introduction of New Birdcage Deformation is a significant advancement in ensuring the safety of nuclear fuel transportation.

4.4 Conclusion of non-uniform arrangement method

Table 4 delineates the positions of the fuel rods along the half of the central axis, offering insight into their spatial arrangement. Figure 17 visually represents the configuration of fuel rods at the point where k_{eff} attains its maximum value for each method. Upon examination of Table 5, it is observed that for the Uniform Arrangement by Blocks, Layer-by-Layer Determination, and the New Birdcage Deformation methods, the 7-th, 8-th, and 9-th fuel rods are nearly in contact. Concurrently, the central pitches in these arrangements approximate the optimal moderating pitch, which is conducive to enhancing reactivity. Comparatively, the k_{eff} values achieved in these three methods surpass those obtained through the Old Birdcage Deformation approach. This observation underscores the efficacy of the revised models for higher reactivity, which is a critical consideration in the safety analysis of nuclear fuel assemblies.

The Uniform Arrangement by Blocks and the Layer-by-Layer Determination methods are capable of achieving higher values of k_{eff}, primarily because their underlying premise is based on an exhaustive enumeration approach. This method is characterized by its thoroughness but may not align with the real-world phenomena. Between these, the

Table 4 Center distance for each fuel rod located on the half of symmetric axis

Layer	Center distance (m)	
	Uniform arrangement by blocks	Layer-by-layer determination
1	0	0
2	1.475×10^{-2}	1.5×10^{-2}
3	2.95×10^{-2}	3×10^{-2}
4	4.425×10^{-2}	4.5×10^{-2}
5	5.9×10^{-2}	6×10^{-2}
6	7.375×10^{-2}	7.5×10^{-2}
7	8.85×10^{-2}	8.76×10^{-2}
8	9.8×10^{-2}	9.8×10^{-2}
9	1.075×10^{-1}	1.075×10^{-1}
	...	
Layer	Center distance (m)	
	Old birdcage deformation	New birdcage deformation
1	0	0
2	1.63×10^{-2}	1.48026×10^{-2}
3	1.13×10^{-2}	2.96044×10^{-2}
4	4.53×10^{-2}	4.44049×10^{-2}
5	5.35×10^{-2}	5.92032×10^{-2}
6	7.12×10^{-2}	7.39987×10^{-2}
7	8.35×10^{-2}	8.85×10^{-2}
8	9.56×10^{-2}	9.8×10^{-2}
9	1.075×10^{-1}	1.075×10^{-1}

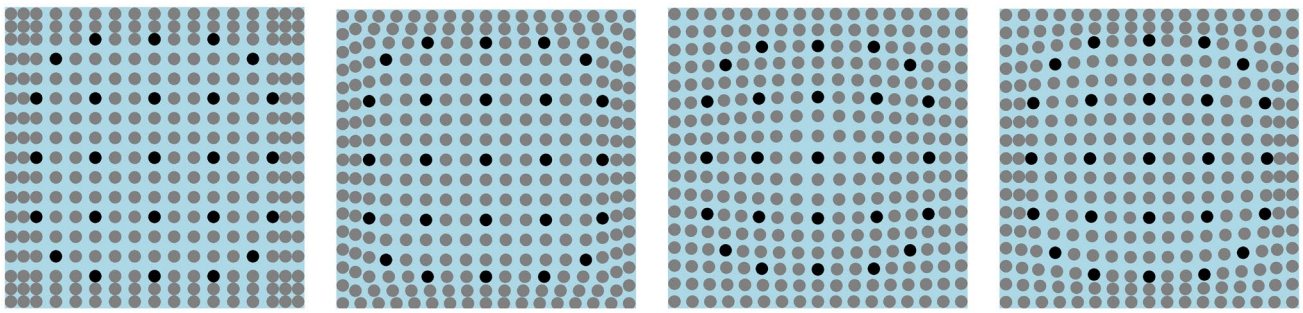

Fig. 17 (Color online) Arrangement when $k_{\text{eff,max,r}}$ of four methods. **a** Uniform Arrangement by Blocks. **b** Layer-by-Layer Determination. **c** Old Birdcage Deformation. **d** New Birdcage Deformation

Layer-by-Layer Determination method is noted for its more conservative approach. In contrast, two Birdcage Deformation methods take a different approach by grounding its analysis in actual observed phenomena. Besides, Sect. 3.C of this study provides compelling evidence that the New Birdcage Deformation model merits consideration when examining the worst-case configurations of fuel rods. The analysis now narrows down to a comparative evaluation between the

Table 5 $k_{\text{eff,max,r}}$ of four methods

Method	$k_{\text{eff,max,r}}$
Uniform Arrangement by Blocks	0.99793
Layer-by-Layer Determination	0.99827
New Birdcage Deformation	0.99650
Old Birdcage Deformation	0.99261

Layer-by-Layer Determination and the New Birdcage Deformation methods (Table 5).

$k_{\mathrm{eff,max,r}}$ derived from the Layer-by-Layer Determination method is distinctly superior to that of the new Birdcage deformation scenario. Nonetheless, in the context of the New Birdcage Deformation, it is imperative to account for the potential to augment $k_{\mathrm{eff,max,r}}$ through subtle variation in the positioning of each fuel rods. As articulated in Ref. [32], these incremental adjustments can lead to a further enhancement of $k_{\mathrm{eff,max,r}}$. Incorporating the effects of these minor rod position perturbations, the revised maximum $k_{\mathrm{eff,max,r}}$ for the New Birdcage Deformation is refined according to the subsequent formula Eq. (15):

$$k_{\mathrm{eff,max,r}} = (1 + E_{\mathrm{s}})k_{\mathrm{eff,max,r}} \tag{15}$$

where $k_{\mathrm{eff,max,r}}$ is $k_{\mathrm{eff,max,r}}$ after revising by small-scale pitch shift, E_{s} is the enhancement amplitude of small-scale pin pitch shift. E_{s} is taken as 0.109% according to Ref. [32]. It is unnecessary to consider the possibility that small-scale pin pitch shift can continue to rise k_{max} obtained by Layer-by-Layer Determination. This is because this method is a kind of enumeration method, which is impossible to occur in an actual accident and it is conservative enough.

5 Method conclusion and example analysis

The research presented in this paper is capable to introduce a method for determining the k_{eff} envelope value for PWR transport containers caused by fuel rods rearrangement in the event of fuel rod mispositioning accidents. This method is universal and can be extended to transport containers for other types of PWR fuel assemblies. The methodology is summarized in the following four steps:

S1: Establishing the Monte Carlo model for an evaluated transport package under accident conditions.
S2: Ascertain the maximum value of k_{eff} attainable by rearranging the fuel rods using the Layer-by-Layer Determination methods.
S3: Employing the New Birdcage Deformation to determine the maximum k_{eff} value achievable through the rearrangement of the fuel assembly.
S4: Revise the maximum k_{eff} value obtained in S3 by Eq. (15) and compare it with the result from S2. The bigger one is the ultimate reactivity envelope value for rods mispositioning accidents.

With the completion of the methodology for determining the envelope model for non-uniform displacements of fuel rods under accident conditions, this research now applies the aforementioned approach to the criticality safety evaluation of a specific model of a AFA3G-type fuel assembly transport cask. The evaluation is conducted within the context of hypothetical accident scenarios to assess the transport cask's safety performance under extreme conditions. A comparative analysis will be undertaken, juxtaposing the results of this research with the existing criticality safety assessment techniques currently employed by the CNPRI for the same class of transport casks. This comparative approach is designed to elucidate the enhancements offered by the new methodology proposed in this paper, particularly in terms of providing a safety margin of safety for criticality safety analysis of fuel transport containers.

The transport cask in question is designed to accommodate two sets of AFA3G-type fuel assemblies at once. The interior walls of the storage cavity are equipped with neutron-absorbing materials, and the cask is intended for use in dry transportation methods. In the event of an accident, the fuel assemblies contained within the cask are envisaged to be entirely inundated by water. The Monte Carlo computational model for the transport cask under accident conditions is illustrated in the designated container section as presented in Fig. 18.

Section 3 provides evidence that the application of the Layer-by-layer Determination method for the non-uniform arrangement of AFA3G-type fuel assemblies can yield the highest possible value of k_{eff}. In light of this finding, the fuel rods of the two sets of AFA3G-type fuel units housed within this transport cask are configured as illustrated in Fig. 17(b). The cross-sectional representation of the Monte Carlo computational model for this specific cask is presented in Fig. 18. The resultant k_{eff} from these calculations is determined to 0.88807, accompanied by a standard deviation of 0.00029.

Currently, in the absence of comprehensive studies on the impact of fuel rod arrangements in the event of accidents,

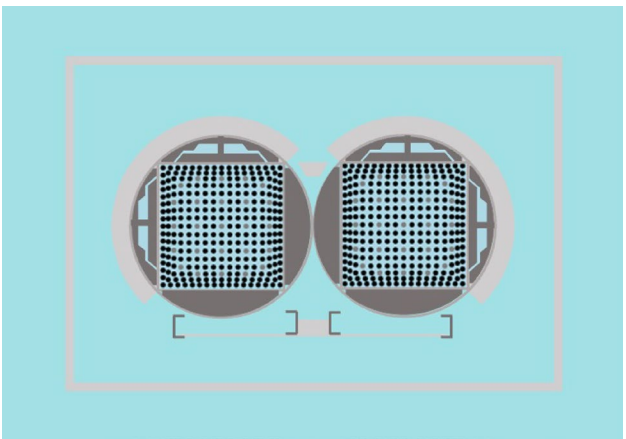

Fig. 18 (Color online) Envelope model for certain AFA3G-Type fuel assembly transport packaging

CNPRI has established a criticality safety assessment protocol. This protocol is based on the maximum value of k_{eff}, obtained from a uniform arrangement of fuel rods within the storage cask, with an additional conservative penalty of 4000 pcm to account for potential accident scenarios. Specifically, when the fuel rods are evenly distributed, the calculated maximum k_{eff} is recorded as 0.87192, accompanied by a standard deviation of 0.00028. The imposition of the 4000 pcm penalty elevates this value to 0.91192, thereby ensuring a heightened level of safety precaution in the criticality assessment of the system under accident conditions.

Upon juxtaposing the assessment methodology established in this research with the extant approaches, it is observed that it confers an approximate increment of 2385 pcm in the criticality safety margin for the evaluation of this specific AFA3G-type fuel assembly transport cask.

6 Conclusion

The research presented in this paper contributes a robust methodological framework and insights of considerable value to the nuclear industry, particularly in the realm of assessing transport containers for fuel assemblies. By employing the methodologies established in this study, it is possible to evaluate the critical safety risks associated with fuel assemblies during accidental conditions with greater precision. This enhanced predictive capability fortifies the assurance of safe nuclear fuel transportation, offering a substantial advancement in the field of nuclear safety protocols.

This research delves into the effects of fuel rod misalignment on criticality safety during transportation accidents by applying three varied methodologies for holistically research on non-uniform fuel rod arrangement. It introduces an envelope determination technique that accounts for a comprehensive range of potential fuel rod misalignment scenarios, thereby providing innovative insights into the criticality safety analysis of fuel assembly transport containers under accident conditions. Notably, the Layer-by-Layer Determination and the New Birdcage Deformation methods excel in increasing the k_{eff}, each from a unique perspective. Therefore, when formulating the envelope model for fuel rod misalignment accidents, a comparative evaluation should be conducted between these two methods to identify the most effective strategy for ensuring criticality safety. The ultimate envelope model presents a significant advancement over traditional criticality safety analysis methods by substantially increasing the safety margin.

While this study has achieved notable advancements at the practical level, there is ample scope for further research. Future work can concentrate on several key areas:

a. An in-depth investigation of the axial deformation of fuel assemblies under impact accidents is necessary to establish a more precise criticality safety analysis model, thereby significantly enhancing the safety margin.
b. It is essential to explore methods for rapidly determining the envelope model for fuel assembly misalignment accidents, aiming to reduce the consumption of computational resources and increase analytical efficiency.
c. The methodology developed in this study should be extended to the criticality safety analysis of other rod-bundle type fuel assembly transport containers under accident conditions, to verify its universality and applicability.

Author contributions All authors contributed to the study conception and design. Material preparation, data collection and analysis were performed by Xin-ling Dai, De-chang Cai, Yan-min Zhang and Jin Cai. The first draft of the manuscript was written by Xin-ling Dai, and all authors commented on previous versions of the manuscript. All authors read and approved the final manuscript.

Data availability The data that support the findings of this study are openly available in Science Data Bank at https://cstr.cn/31253.11.sciencedb.j00186.00840 and https://www.doi.org/10.57760/sciencedb.j00186.00840.

Declarations

Conflict of interest The authors declare that they have no Conflict of interest.

References

1. C. Wang, X. Chai, B. Yang et al., Development and prospect of advanced nuclear energy technology. Energy Technol-Ger. Nuclear Power Eng. **44**, 5 (2023). https://doi.org/10.13832/j.jnpe.2023.05.0001
2. Y. Dong, G. Li, Y. Qu, Analysis on several problems of Nucl. Energy development from Nucl. Safety. Environ. Prot. **45**, 36–40 (2017). https://doi.org/10.14026/j.cnki.0253-9705.2017.18.007
3. International Atom. Energy+ Agency, *Regulations for the safe transport of radioactive material*. (IAEA Safety Standards Series No. TS-R-1, Vienna, 2005). https://doi.org/10.61092/iaea.ur52-my9o
4. Ministry of Ecol. Envir. of People's Republic of China, *Regulations for the safe transport of radioactive material*. (Standardization Administration of the People's Republic of China, 2019). https://www.mee.gov.cn/ywgz/fgbz/bz/bzwb/hxxhj/fsxhjbz/201903/W020190322511199923924.pdf
5. Y. Li, D. Xiao, X. Liu et al., Discussion on the present situation of spent fuel transportation in China. Radiat. Prot. **36**, 1 (2016) https://tinyurl.com/ms2vc7cy
6. R. Zhou, J. Qian, Challenges and recommendations for the back end of the nuclear fuel cycle in China. China Nucl. Ind. **10**, 27–29 (2013) https://tinyurl.com/4e8d38dk
7. C. Ma, Exploration of the main problems and basic countermeasures in the safety regulation of the transport of radioactive materials in China. Paper presented at the 4th Forum on Radiat. Prot. at the beginning of the 21st century and symposium on

low-intermediate-range waste manage. and transport of radioactive substances, Beijing, (2005). https://tinyurl.com/5xrdnjke
8. X. Li, Study on certain issues in the construction and practice of the spent fuel transport system in China. Paper presented at the 4th forum on radiat. prot. at the beginning of the 21st century and symposium on low-intermediate-range waste manage. and transport of radioactive substances, Beijing, (2005). https://tinyurl.com/u763vn2c
9. Q. Sun, D. Zhuang, H. Sun et al., Overview of application status for nuclear fuel assembly transport package. Packag. Eng. **43**, 142–150 (2022). https://doi.org/10.19554/j.cnki.1001-3563.2022.13.018https://d.wanfangdata.com.cn/periodical/bzgc202213019
10. G. Li, B. Zhao, J. Zhang et al., Test for radioactive material transport package safety. Atom. Energy Sci. Technol. **Suppl.**, 668–670 (2012). https://tinyurl.com/bddmy3bd (in Chinese)
11. Y. Zhou, Review of design and experimentation of type RY-I spent fuel transport package. Radiat. Prot. Bulletin. **5**, 51–58 (1991) https://tinyurl.com/5t4sva7n
12. G. Li, J. Zhang, B. Zhao et al., Test of type FCo70-YQ transport container for medical radioactive source in CIRP. Prog. Nucl. Sci. Technol. **1**, 456–459 (2011). https://doi.org/10.15669/pnst.1.456
13. X. Yi, X. Huo, Consideration in criticality safety evaluation of transport package. Atom. Energy Sci. Technol. **Suppl.**, 309–311 (2013). https://doi.org/10.7538/yzk.2013.47.S0.0309https://d.wanfangdata.com.cn/periodical/yznkxjs2013z1071 (in Chinese)
14. Z. Xie, *Physical Analysis of Nuclear Reactors*. (Atom. Energy+ Press, Shaanxi, 2004), pp. 89–111. https://tinyurl.com/56tnssfj
15. J.J. Duderstadt, L.J. Hamilton, *Nuclear Reactor Analysis* (Wiley, New York, 1976) https://hdl.handle.net/2027.42/89079
16. G.A. Schlapper, Methods of steady-state reactor physics in nuclear design. Nucl. Technol. **65**, 358 (1984). https://doi.org/10.13182/NT84-A33423
17. F. Wang, J. Lang, X. Tan et al., Comparative analysis of physical characteristics of coolant/moderator material used in micro-nuclear reactor. Highlight Sciencepaper Online **16**, 138–143 (2023). https://doi.org/10.3969/j.issn.1674-2850.2023.01.015
18. S. Qiang, Q. Yin, W. Lu et al., Sensitivity analysis of nuclear data in core critical calculation of Qinshan II. High Power Laser Part. Beams **29**, 3 (2017). https://doi.org/10.11884/HPLPB201729.160433
19. State General Administration of the People's Republic of China for Quality Supervision and Inspection and Quarantine, *Nuclear criticality safety for fissile materials outside reactors – Part 8: criticality safety criteria for the handling storage and transportation of LWR fuel outside reactors*. (Standardization Administration of the People's Republic of China, 2008). https://openstd.samr.gov.cn/bzgk/gb/newGbInfo?hcno=6854BAFC1D378AAE9D5C61741C999953
20. L. Zhang, B. Zhao, X. Wang et al., Progress in demonstration test for radioactive material transport packages. Radiat. Prot. **30**, 6 (2010). https://doi.org/10.3969/j.issn.1004-6356.2010.06.001
21. H. Li, Z. Sun, S. Sun et al., Drop impact analysis method of radioactive material container. Nucl. Tech. **4**, 343–346 (2013) https://tinyurl.com/3ypeetzf
22. X. Xu, B. Zhao, J. Zhang et al., Drop test using finite element method for transport package of radioactive material. Atom. Energy Sci. Technol. **3**, 381–384 (2010). https://doi.org/10.7538/yzk.2010.44.03.0381
23. P.P. Millán, C. Vaughan, B. Gogolin, Drop test for the licensing of the RA-3D package in the transport of BWR fresh fuel assemblies. Paper presented at 13th international symposium on the packaging and transportation of radioactive materials, Chicago, (2001). http://resources.inmm.org/system/files/patram_proceedings/2001/33449.PDF
24. B. Gogolin, B. Droste, P.P. Millán, Drop tests with the RA-3D shipping container for the transport of fresh BWR fuel assemblies. Paper presented at 13th international symposium on the packaging and transportation of radioactive materials, Chicago, (2001). http://resources.inmm.org/system/files/patram_proceedings/2001/33403.PDF
25. Q. Xiang, L. Han, Research on the application of wire rope isolator buffer device in the transportation of nuclear fuel asemblies. Electric. Eng. **3**, 161–164 (2023). https://doi.org/10.19768/j.cnki.dgjs.2023.03.040
26. A.H. Wells, A. Machiels, Effects of fuel relocation for transport casks. Nucl. Technol. **179**, 180–188 (2017). https://doi.org/10.13182/NT84-A33423. https://doi.org/10.13182/NT12-A14090
27. P. C. Purcell, Method to evaluate limits of lattice expansion in light water reactor fuel from an axial impact accident during transport. Paper presented at the 15th international symposium on the packaging and transportation of radioactive materials, Florida, (2007). https://resources.inmm.org/system/files/patram_proceedings/2007/310.pdf
28. X. Wang, D. Zhu, G. Li et al., Criticality safety analysis to transport package of intact AP1000 fuel assembly. Radiat. Prot. **34**, 97–101 (2014). https://doi.org/10.3969/j.issn.1000-8187.2014.02.006. https://kns.cnki.net/kcms2/article/abstract?v=BlOUhu2v8Y_kucfmpXT5kgiIArX6FLJepa7BpaEX1Fxe5rO29uSJ4Miju6YSLk4AjkHGRas_xtAyGIg3sLTJdIQpj8f7O3kpxqHRFvvXKxSQ4d-4ewfccd1OwEH6-Uzd_wsmxSn5-PJelX5ZE4iGSTOX6wjJHSG&uniplatform=NZKPT
29. W.B.J. Marshall, J.C. Wagner, Consequences of fuel failure on criticality safety of used nuclear fuel. Oak Ridge National Lab, No. ORNL/TM-2012/325. https://info.ornl.gov/sites/publications/files/Pub38136.pdf
30. C. Xu, Research on key technologies for spent fuel transport containers based on safety analysis, Zhejiang University, (2012). https://tinyurl.com/nhzveu5b
31. L. Whittingham, L.M. Farrington, M.A. Peers, Effects of impact accidents on transport criticality safety cases for LWR packages-a new approach. Paper presented at the 13th international symposium on the packaging and transportation of radioactive materials, Chicago, (2001). https://resources.inmm.org/system/files/patram_proceedings/2001/33534.PDF
32. M. Asami, N. Odano, New approach to evaluate lattice expansion of light water reactor fuel elements on criticality safety of transport packages under impact accidents. Packag. Transp. Storage Secur. Radioact. Mater. **212**, 80–90 (2013). https://doi.org/10.1179/174650910X12665760844431
33. Y. Li, H. Yang, X. Yi et al., Benchmark experiment and analysis of JMCT on nuclear critical safety. High Power Laser Part. Beams. **1**, 29 (2017). https://doi.org/10.11884/HPLPB201729.160212
34. R.Y. Rubinstein, D.P. Kroese, *Simulation and the Monte Carlo method*. (Wiley, 2016), p. 1. https://doi.org/10.1002/9781118631980
35. American Nuclear Society, *Nuclear criticality safety in operations with fissionable material outside reactors*. (American National Standard, Illinois, 1998). https://www.nrc.gov/docs/ML0037/ML003726480.pdf
36. American Nuclear Society, *Validation of neutron transport methods for nuclear criticality safety calculations. American Nuclear Society*. (American National Standard, Illinois, 2007). https://www.ans.org/store/peek/item-240320
37. B.C. Kiedrowski, F.B. Brown, J.L. Conlin et al., Whisper: sensitivity/uncertainty-based computational methods and software for determining baseline upper subcritical limits. Nucl. Sci. Eng. **1**, 17–47 (2017). https://doi.org/10.13182/NSE14-99
38. Z. Li, M. Rahimi, D. Tang et al., Regulatory perspective on potential fuel reconfiguration and its implication to high burnup spent fuel storage and transportation. Paper presented at WM2013

conference, Phoenix, Arizona, USA, (2013). https://www.osti.gov/biblio/22224844
39. I. Reiche, Influence of the accident behaviour of spent fuel elements on criticality safety of transport packages–some basic considerations. Paper presented at the 15th international symposium on the packaging and transportation of radioactive materials, Florida, (2007). https://resources.inmm.org/system/files/patram_proceedings/2007/128.pdf
40. L.E. Beghian, N.C. Rasmussen, R. Thews et al., The investigation of neutron kinetics and cross section in fast nonmoderating assemblies by the nanosecond pulsed neutron source technique. Nucl. Sci. Eng. **4**, 375–381 (1963). https://doi.org/10.13182/NSE63-A26453
41. J.M. Scaglione, G. Radulescu, W.J. Marshall et al., A quantitative impact assessment of hypothetical spent fuel reconfiguration in spent fuel storage casks and transportation packages. Oak Ridge National Lab, No. ORNL/TN 37831-6170. https://www.nrc.gov/docs/ML1511/ML15119A240.pdf